Environ Fluid Mech (2014) 14:821–847
DOI 10.1007/s10652-013-9332-1

ORIGINAL ARTICLE

Three-dimensional analysis of coherent turbulent flow structure around a single circular bridge pier

Alireza Keshavarzi · Bruce Melville · James Ball

Received: 24 March 2013 / Accepted: 24 December 2013 / Published online: 17 January 2014

Abstract The coherent turbulent flow around a single circular bridge pier and its effects on the bed scouring pattern is investigated in this study. The coherent turbulent flow and associated shear stresses play a major role in sediment entrainment from the bed particularly around a bridge pier where complex vortex structures exist. The conventional two-dimensional quadrant analysis of the bursting process is unable to define sediment entrainment, particularly where fully three-dimensional flow structures exist. In this paper, three-dimensional octant analysis was used to improve understanding of the role of bursting events in the process of particle entrainment. In this study, the three-dimensional velocity of flow was measured at 102 points near the bed of an open channel using an Acoustic Doppler Velocity meter (Micro-ADV). The pattern of bed scouring was measured during the experiment. The velocity data were analysed using the Markov process to investigate the sequential occurrence of bursting events and to determine the transition probability of the bursting events. The results showed that external sweep and internal ejection events were an effective mechanism for sediment entrainment around a single circular bridge pier. The results are useful in understanding scour patterns around bridge piers.

Keywords Transition probability · Bursting process · Bridge pier · Scouring

A. Keshavarzi (✉) · J. Ball
School of Civil and Environmental Engineering, F.E.I.T., University of Technology Sydney, Broadway, NSW 2007, Australia
e-mail: alireza.keshavarzi@uts.edu.au

A. Keshavarzi
Water Department, Shiraz University, Shiraz 7144, Iran

B. Melville
Department of Civil and Environmental Engineering, The University of Auckland, Auckland, New Zealand

1 Introduction

The problem of local scouring around a bridge pier has received much attention, due to the possibility of severe damage occurring to the bridge during flood events [1–4]. The flow around a bridge pier is fully three-dimensional, comprising a complex vortex motion [5–10]. The mechanism of local scouring around bridge piers is basically the result of the down flow direction upstream of the pier and vortex generation at the bed. The down flow impacts on the bed material and creates a scour hole in the vicinity of the pier [6,8,10–13]. Figure 1a shows the down flow mechanism, vortices and scouring pattern around a circular bridge pier. The upstream vortex is called a horseshoe vortex and is highly effective for movement of sediment particles away from the pier. In addition to the horseshoe vortex, there are wake vortices downstream of the pier, which are shed sequentially from one side to other side of the pier (Fig. 1b, c). Both the horseshoe vortex and the wake vortices are responsible for entrainment of sediment particles from the bed [6,14]. As a result, a scouring process gradually develops around the pier whereas sediment deposition occurs further downstream

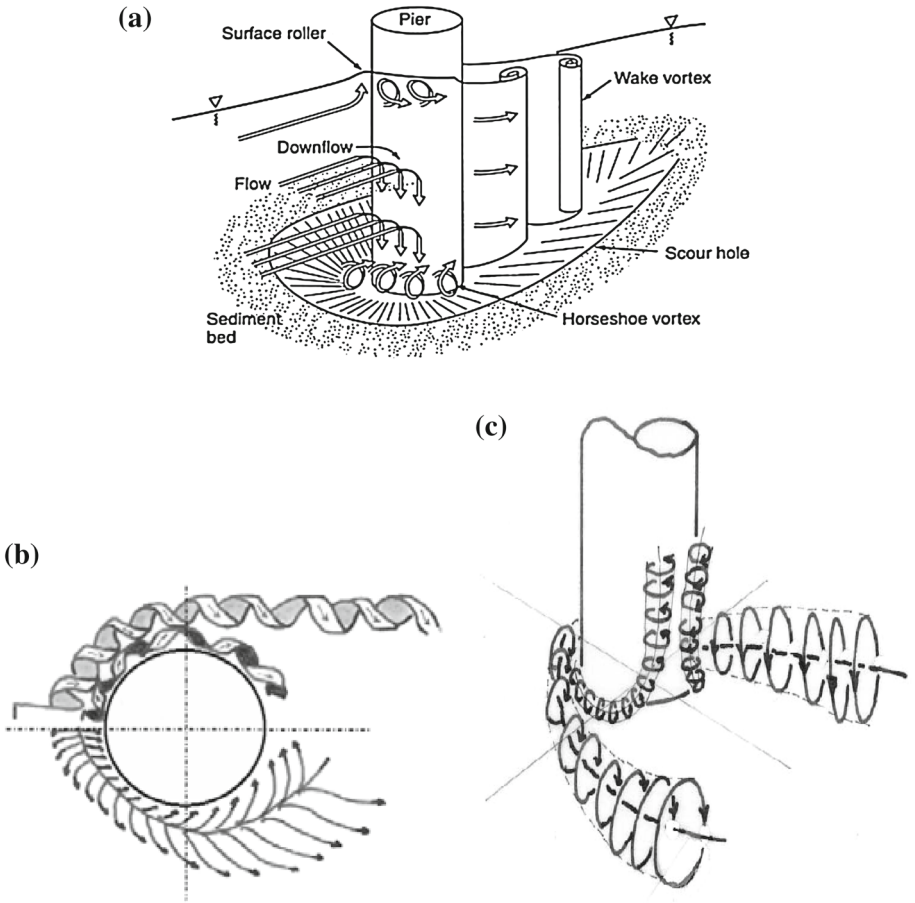

Fig. 1 **a** Flow mechanism and scour pattern around a circular bridge pier [2], **b** flow image (Tsutsui 2002) and **c** horseshoe vortex system (Tsutsui 2002)

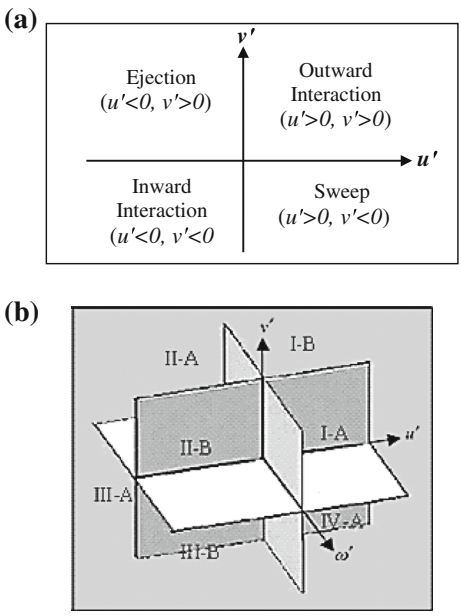

Fig. 2 **a** Quadrant analyse of two-dimensional velocity fluctuations. **b** Three-dimensional view of two classes of bursting events and eight associated orthogonal zones [17]

of the pier. In most of the previous studies attention has been paid to develop scour–depth relationships, rather than to assess how coherent turbulent flow affects the mechanism of local scouring. In order to define the scouring mechanism, the turbulent flow field must be understood before the bed scouring process.

The inherent temporal organization of bursting events consists of the movements from one situation to another with time. The bursting phenomena are quasi-periodic organized processes which occur randomly in time and place in the quadrant zones presented in Fig. 2a [15]. The situation of bursting events at any particular time is very important for particle entrainment and produces local intermittent erosion and deposition. The study by Hussain [16] showed that a coherent structure is a large conglomeration of turbulent eddies which has a fundamental sense of rotation and the bursting processes are the evolution of coherent turbulent flow structures during their birth, growth and successive breakdown. Thus, the bursting events are spatio-temporal in nature and quadrant analysis of two-dimensional velocity fluctuations may reduce the resolution of the results.

According to quadrant analysis of the bursting process, ejection events are associated with low speed fluid moving from the boundary layer into the main flow, extending the turbulent shear layer towards the water surface. Sweep events represent high speed fluid motion from the main flow into the boundary layer with a downward direction [18–21]. Therefore, close to the bed, sweeps produce several small-scale eddies created in the strong turbulent shear layer [22]. Outward interaction events produce high velocity pulses from the boundary into the main flow towards the water surface and in the direction of flow, whereas inward interactions generate low velocity pulses from the main flow into the bed in a direction opposite to the main flow direction [21].

Thorne et al. [23], Townsend [24] and Nezu and Nakagawa [25] used quadrant analysis of the bursting process and have shown that the time fraction of sweep and ejection events is more than that of outward and inward interactions. Therefore, the different bursting events have different influences on the mode and rate of sediment transport [26]. Keshavarzi and Ball [27] pointed out that in sweep events, the average magnitude of the shear stress is more than

two times that of the overall time averaged shear stresses. Nakagawa and Nezu [28], Grass [29], Nychas et al. [30], Offen and Kline [18] found that sweep events become more important than ejection events with increasing bed roughness. Furthermore, Keshavarzi et al. [31] investigated the dominant bursting events and the flow structure over ripples in the bed of a channel and they found that downstream of the second ripple, bursting events were dominant in quadrants 1 and 3 whereas upstream of the ripple, they were dominant in quadrants 2 and 4. Their results also showed that the occurrence probabilities of sweep events along the channel bed are in phase with the bed forms, whereas those of ejection events are out of phase with the bed forms. To define the stochastic nature of the bursting process and sequential occurrence of bursting events, Keshavarzi and Shirvani [32] defined three organized movements in sequential time series occurrence of bursting process and found that stable organizations is the most probable events. Therefore, in this study, the stable transition probability of the bursting events and their effect on bed scouring were investigated in this study.

In general, using quadrant analysis for open channel flow, the sweep event was found to be an important event for entrainment of particles from the bed surface. The studies by, for example, Thorne et al. [23], Nelson et al. [33], Drake et al. [34], Keshavarzi and Ball [35] and Cuthbertson and Ervine [36], investigated 2-D quadrant analysis of the bursting process and indicated that close to the bed most of the sediment entrainment occurs during sweep events. In particular, Marchioli and Soldati [37], and Dwivedi at al. [38,39] found that coarse sediment particles were entrained during sweep events.

However, the flow around bridge piers is fully 3-D, hence 2-D analysis of the bursting process cannot clearly define the entrainment process. Therefore, the technique used in this study provides more resolution to the effect of transverse velocity fluctuations in the entrainment process. Using the above technique, the sweep events were categorized into external and internal zones depending on the sign of the transverse velocity fluctuations. In this study, the flow around one single column circular bridge was investigated. The bridge pier produces a contraction to the flow and diverts flow from the centreline of the flow to the sides of the flume. Therefore, the flow diverted to the sides may also contribute a component of external ejection to the entrainment process.

The studies by Keshavarzi and Gheisi [17] also showed that two-dimensional analysis of bursting analysis is unable to define entrainment process when there is fully three-dimensional flow in nature. They developed a method of three-dimensional octant analysis to account the effect of secondary flow. In this study, to investigate the coherent turbulent flow structure around bridge pier, the above technique was used to analyse measured experimental velocity data.

The classifications of bursting events were performed based on the sign of the velocity fluctuations in three dimensions. The velocity fluctuations are defined by:

$$u' = u_i - \overline{u}, \quad v' = v_i - \overline{v} \text{ and } w' = w - \overline{w} \tag{1}$$

where

$$\overline{u} = \frac{1}{n}\sum_{i=1}^{n} u_i, \overline{v} = \frac{1}{n}\sum_{i=1}^{n} v_i \text{ and } \overline{w} = \frac{1}{n}\sum_{i=1}^{n} w_i. \tag{2}$$

The u' and v' and w' are the velocity fluctuations or deviation of velocity from the time-averaged velocity at a point in the flow, in the streamwise (x), vertical (z) and transverse (y) directions (Fig. 2b). The u_i, v_i and w_i are the instantaneous velocities and $\bar{u}$, $\bar{v}$ and $\bar{w}$ are the temporal averaged velocities in the streamwise, vertical and transverse directions, respectively, and n is the number of instantaneous velocity samples.

Table 1 Three-dimensional analysis of bursting events (Group A and Group B for left side of channel)

Classes of bursting evens in Group A	Sign of fluctuating velocities		
	u'	v'	w'
Class I-A (internal outward interaction)	+	+	+
Class II-A (internal ejection)	−	+	−
Class III-A (internal inward interaction)	−	−	−
Class IV-A (internal sweep)	+	−	+
Classes of bursting evens in Group B	Sign of fluctuating velocities		
	u'	v'	w'
Class I-B (external outward interactions)	+	+	−
Class II-B (external ejection)	−	+	+
Class III-B (external inward interaction)	−	−	+
Class IV-B (external sweep)	+	−	−

As presented in Table 1, the three-dimensional bursting process is classified into internal (Class A) and external (Class B) events. The definitions of the eight orthogonals into internal and external events are based on diagonal, rather than side-by-side boundaries.

Based on the above classification, the bursting events are classified into eight orthogonal zones of the events as:

(i) Internal outward interaction or class I-A, ($u' > 0, v' > 0, w' > 0$);
(ii) Internal ejection or class II-A, ($u' < 0, v' > 0, w' < 0$);
(iii) Internal inward interaction or class III-A, ($u' < 0, v' < 0, w' < 0$);
(iv) Internal sweep or class IV-A, ($u' > 0, v' < 0, w' > 0$);
(v) External outward interaction or class I-B, ($u' > 0, v' > 0, w' < 0$);
(vi) External ejection or class II-B, ($u' < 0, v' > 0, w' > 0$);
(vii) External inward interaction or class III-B, ($u' < 0, v' < 0, w' > 0$); and
(viii) External sweep or class IV-B, ($u' > 0, v' < 0, w' < 0$).

These are shown schematically in Fig. 2b.

The difference between internal and external sweep events can be recognized through 3-D vortex rotations. The secondary flow at each cross section induced by flow velocity in the transverse direction is not negligible in three-dimensional flow. As a result two vortices exist that rotate in clockwise and anticlockwise directions (Fig. 1b, c). The internal sweep vortex rotates in the clockwise direction, while the external sweep event rotates in the anti-clockwise direction. Thus the two vortices move sediment particles in different directions. In two-dimensional quadrant analysis of the bursting process, there is no distinction between clockwise and anticlockwise vortex motion.

The importance of this study is that most of the previous studies focused on two-dimensional quadrant analysis of fluctuating velocities in open-channel flow, whereas the flow structure in rivers and natural channels are three-dimensional coherent turbulent structures. Therefore, the velocity in the transverse direction could not be neglected, inducing a secondary circulating flow at the cross section. The developed method of three-dimensional

octant analysis enables the effect of secondary flow to be taken account of. In this paper, to investigate the coherent turbulent flow structure around bridge piers, experiments were conducted with the intention of obtaining the contribution of eight different bursting events.

Therefore, the three-dimensional analysis of bursting processes was used to find the characteristics of turbulent flow around a single bridge pier. The turbulent flow characteristics of the eight bursting events around a single circular bridge pier are investigated in association with the corresponding scouring pattern. The importance of internal and external bursting events on sediment particles movement and their relations with bed scouring are presented in this paper.

2 Experimental setup

The experiments were performed in a flume of 15 m long, 0.7 m wide and 0.6 m deep. The bed of the flume was filled to a depth of 120 mm with a uniform sand of median size $D_{50} = 0.63$ mm . A cylindrical bridge pier of diameter 50 mm was installed at the centre of flume. The coordinates of the pier location are $x = 0$, $y = 0$ as they are shown in all drawings. The position $x = 0$ is the centre of pier and $y = 0$ is the centre line of the flume. The ratio of the flume width to pier diameter was 14, such that any side wall effects were eliminated [5]. The ratio of pier diameter to sediment size was 79, such that sediment size effects were also not present [40].

The experiments, which were carried out under two different conditions (fixed bed and movable bed), were: (a) Test 1 (Fixed bed) with flow rate = 13.6 l/s, flow depth = 160 mm, mean velocity = 0.12 m/s, Froude number = 0.096 and Reynolds number = 19,360 and (b) Test 2 (Movable bed) with flow rate = 25 l/s, flow depth = 97 mm, mean velocity = 0.377 m/s, Froude number = 0.368 and Reynolds number = 35,714.

The sandy surface meter (WH-406) was used to measure the bed profile and bed scouring pattern around the bridge pier. The scouring was measured at the end of each experimental test along lines A, B and C from upstream to downstream of the pier after achieving the equilibrium condition (Fig. 3a, b). The scoured bed profiles along lines A, B and C are shown in Fig. 4a, where the zero level is the floor of the flume and 120 mm is the top level of the sediment layer. Maximum scouring depth can be seen at line A at location about 40 mm upstream which is consistent with previous studies [2,12]. To compare the bed elevation with other flow characteristics in the next sections, the contour plot of bed topography is presented in Fig. 4b. The blue colour is the lowest bed elevation where maximum scouring hole occurred and red colour is the highest bed elevation with minimum scouring. The water surface inside the flume was controlled using a downstream gate. A pre-calibrated V-Notch weir installed at the downstream end of the flume with an electromagnetic flow meter installed in the inlet pipe were used to measure the accuracy of flow rate during the tests.

2.1 Three-dimensional velocity measurement

The velocity fluctuations in the flow were measured to an accuracy of +/− 0.1 m/s at a frequency of 50 Hz in three dimensions using a down-looking Acoustic Doppler Velocity meter (Micro-ADV) [41]. The duration of sampling at each point of flow was 120 s, such that 6,000 data samples were captured for each velocity component. The velocities were measured at 102 different nodal points, as shown in six different lines in Fig. 3b. After achieving equilibrium conditions, the ADV probe was set at 65 mm above the bed and the velocities were measured in a control volume located at height 15 mm layer above the bed.

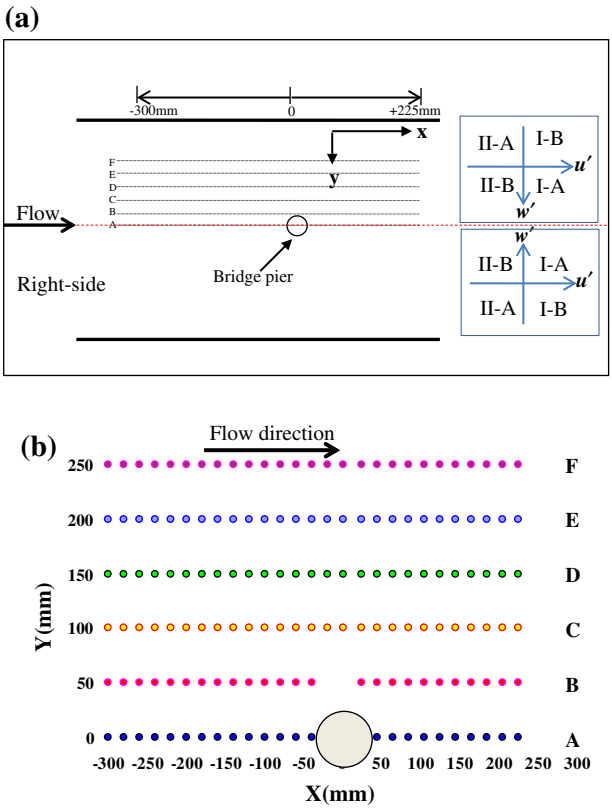

Fig. 3 Coordinate systems **a** lines of measurement for the bed topography and velocity and **b** nodal points of the velocity measurement

The Micro-ADV uses the sound technique to measure the velocity of small particles in the water. The ADV sensor consists of one transmitting transducer and three receiving transducers mounted at 120° azimuth intervals and operates on a pulse-to-pulse coherent doppler shift to measure three-dimensional velocity components. The advantages of using an ADV are that it is capable of measuring three-dimensional velocity components simultaneously, it introduces minimal disturbance to the flow because the sampling volume is 5 cm down from the probe and no calibration is required.

To capture accurate data, the water salinity and temperature were checked during the experiments since the accuracy of the Micro-ADV measurements is acceptable (±0.1 mm/s in full scale) if the two above parameters are correctly determined. The water temperature was measured frequently during the experimental tests and entered into the data acquisition software if any change in water temperature was observed.

To control the accuracy of velocity data, two key parameters, signal to noise ratio (SNR) and correlation coefficient (COR), should be checked. The best ranges of SNR and the COR for reporting good velocity data are greater than 15 dB and 70 %, respectively. In the present experiments, all the reported SNR and correlations were checked at the beginning of each experiment and found to be within the acceptable ranges [41]. The recorded average SNR values ranged from 24 to 26 with the COR 82–98.

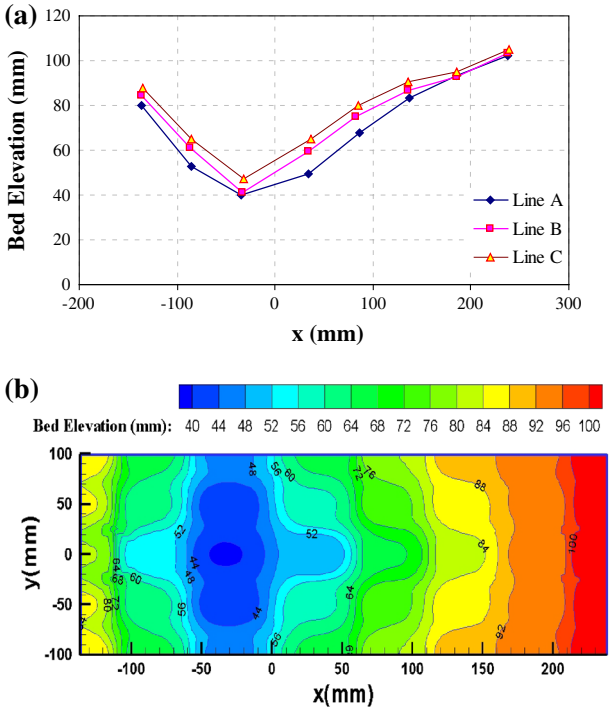

Fig. 4 **a** Scour profile around bridge pier and along lines A, B and C, **b** contour plot of bed elevation around the bridge pier

The noise in Micro-ADV data is the spikes produced by the phase shift ambiguities between the transmitting and receiving pulses. A spike may be produced when the flow velocity exceeds the upper limit of the ADV probe velocity range, or when there is contamination from previous pulses reflected from the boundaries, or when there is highly aerated turbulent flow. To remove noise, the output data from the ADV were filtered using the Phase space threshold despiking filtering. This filter was first suggested by Goring and Nikora [42] and it has implemented in the WinADV Software [43].

3 Results and discussions

In the present study, three-dimensional analyses of the bursting process are used to classify the bursting events [17]. The transition probabilities, occurrence probabilities and inclination angles of three-dimensional bursting events are presented. Then, the measured turbulent flow characteristics, scouring profile, contours of bed topography, kinetic energy, and Reynolds shear stress at different locations upstream and downstream of the pier are discussed.

3.1 Flow characteristics upstream and downstream of the bridge pier

Turbulent kinetic energy of the flow is computed as:

$$\mathrm{TKE}_{\mathrm{xyz}} = \frac{1}{2}\left(\overline{u'^2} + \overline{v'^2} + \overline{w'^2}\right) \tag{3}$$

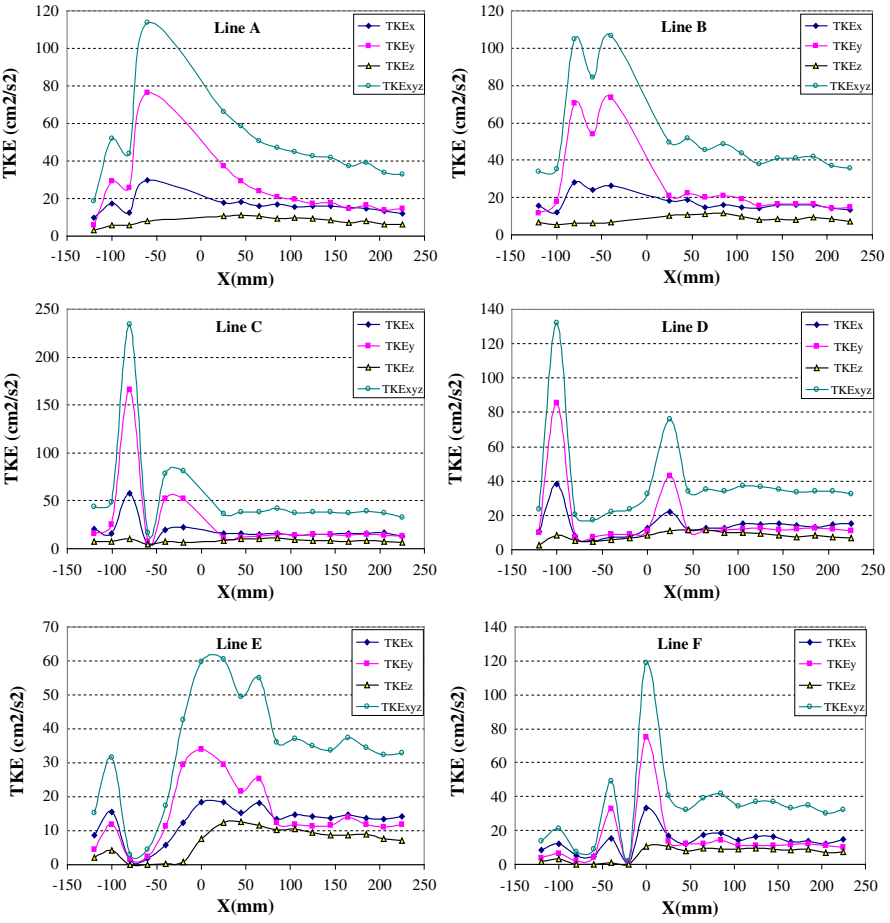

Fig. 5 Variation of TKE in longitudinal profile for movable bed

where TKE_{xyz} is total turbulent kinetic energy of the flow in three dimensions. The magnitude of turbulent kinetic energy for each individual direction was computed for comparison with total turbulent kinetic energy. For the movable bed experiment, the variations of the TKE in x, y and z directions with the total kinetic energy TKExyz are presented in Fig. 5 for different lines (A–F) from upstream to downstream of the bridge pier. The results indicate that TKE varies significantly from upstream to downstream of the pier. At lines A, B and C, the maximum magnitude of TKE is observed at upstream locations where maximum scouring depth occurred (Fig. 4). Therefore, the TKE results are consistent with longitudinal bed scouring for lines A, B and C. At lines E and F which are more distant from the centreline, maximum TKE occurs downstream of the pier.

To compare the contribution to the TKE_{xyz} of different velocity fluctuations (u', v' and w' in x, y and z directions, respectively), average turbulent energy for each line (A–F) is presented in Fig. 6a, b and Table 2, for locations upstream and downstream of the pier, respectively. Comparing the magnitude of TKE in each direction with TKE_{xyz}, it can be concluded that the maximum value of TKE_{xyz} occurred upstream of the pier. The TKE at each flow direction upstream of pier varies significantly from centreline to the side wall,

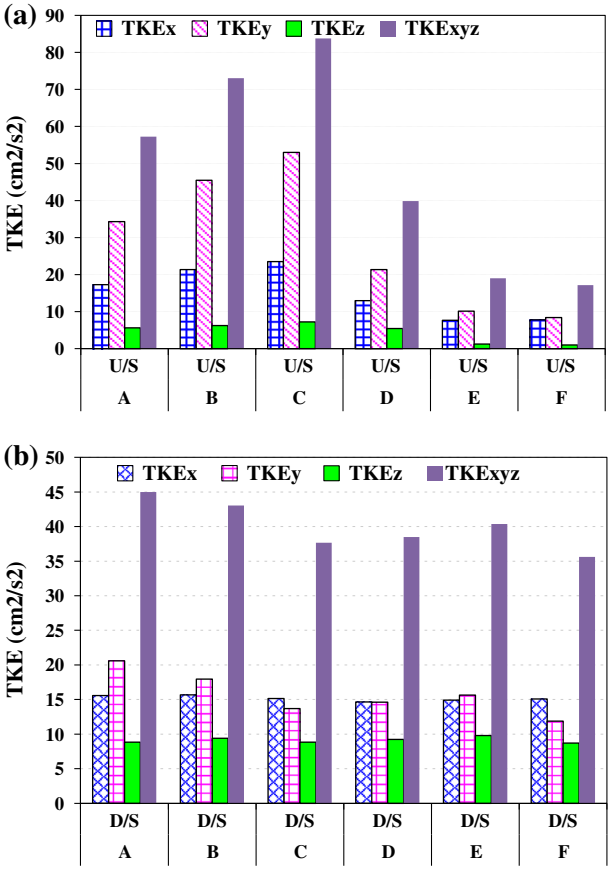

Fig. 6 Averaged longitudinal TKE for upstream and downstream of the pier

however for downstream of the pier, no significant changes for TKE was found. From Table 2, maximum percentage of contribution was found for transverse velocity at location upstream of the pier which is twice the contribution of streamwise direction. Downstream of the pier, again the contribution of transverse velocity direction is higher than streamwise and vertical directions. The contribution of vertical flow direction into total kinetic energy is low when comparing to streamwise and lateral directions. Therefore, it can be speculated that the effect of transverse velocity direction on sediment entrainmnet is higher than streamwise and vertical velocity directions at upstream and downstream of the pier. Based on the above results, the effect of transverse velocity fluctuations can not be neglectted into bursting analysis for the flow around bridge pier.

Contour lines of TKExyz are presented in Fig. 7a. At the locations where the streamwise velocity is sharply diverted in the transverse direction, a high shear layer will be created [9,44]. At such locations, the flow is highly turbulent, for example the blue area in Fig. 7a and high magnitudes of TKE are expected, for example the red area in Fig. 7b [9]. Comparing Reynolds shear stress and turbulent kinetic energy upstream of the pier for the red and blue areas, a steep gradient of shear stress and turbulent kinetic energy is apparent. Similar results were found for lines A, B and C upstream of the pier as the magnitudes of TKExyz are high in those locations. The high magnitudes of shear stress are located in highly turbulent

Table 2 Turbulent kinetic energy of flow for upstream and downstream of pier for movable bed

Lines	Locations	TKE_x	% contribution	TKE_y	% contribution	TKE_z	% contribution	TKE_{xyz}
A	U/S	17.32	30.27	34.29	59.95	5.61	9.81	57.22
B	U/S	21.34	29.21	45.49	62.27	6.23	8.52	73.06
C	U/S	23.50	28.07	52.97	63.26	7.26	8.67	83.74
D	U/S	12.99	32.60	21.38	53.67	5.47	13.73	39.85
E	U/S	7.65	40.16	10.14	53.26	1.25	6.59	19.04
F	U/S	7.79	45.41	8.38	48.90	0.98	5.71	17.15
Average			34.29 %		56.88 %		8.84 %	
A	D/S	15.58	34.62	20.59	45.77	8.83	19.62	45.00
B	D/S	15.68	36.44	17.96	41.74	9.39	21.82	43.03
C	D/S	15.15	40.22	13.69	36.34	8.83	23.44	37.67
D	D/S	14.64	38.06	14.60	37.96	9.23	23.98	38.47
E	D/S	14.92	36.95	15.65	38.77	9.79	24.26	40.37
F	D/S	15.06	42.27	11.87	33.31	8.70	24.42	35.63
Average			38.09 %		39.00 %		22.93 %	

zones and being negative in sweep or ejection zones. The above results are consistent with the observation of horseshoe vortex oscillation around bridge pier [45–47]. Therefore, it can be concluded that moving from one point to another in the transverse direction, the flow situation differs significantly due to fully three-dimensional vortex rotations. The scour pattern (Fig. 4b) confirms that higher bed elevation occurred where minimum shear stress and kinetic energy are measured. In this study, to investigate the spatio-temporal variation of flow characteristics, at a higher resolution, three-dimensional decomposition of bursting events was used.

3.2 Three-dimensional decomposition of bursting events

All of the previous studies for example [15,23,30–35,38,39,48–51] focused on quadrant analysis of two-dimensional velocity fluctuations for different boundary conditions in open-channel flow. However, the flow structure in rivers and natural channels are coherently structured in three dimensions particularly where an obstruction is placed into the flow. The velocity in the transverse direction cannot be neglected, because it can induce significant secondary circulation. Referring to Fig. 1b, c, the two vortices rotating in the clockwise and anticlockwise directions cause aggradation and degradation at the bed [6]. For this study, the method developed by Keshavarzi and Gheisi, [17] was used to classify the three-dimensional bursting events.

Esfahani and Keshavarzi [52,53] and Liu and Bai [54] used the above concept and technique to understand the mechanism of the bursting process in a meandering channel. They found that the above technique provided more resolution to the understanding of coherent flow structures and their influences on sediment entrainment in meanders.

Based on the above technique, the events are classified into two clusters including eight orthogonal zones which are occurring temporally in spatial zones of 1, 2, 3,…,8, respectively. Classification of the clusters is based on sign of the velocity fluctuations in streamwise, vertical and transverse directions (Table 1). Cluster A indicates the group of events in which their deflections are towards the internal or centreline direction and cluster B indicates the

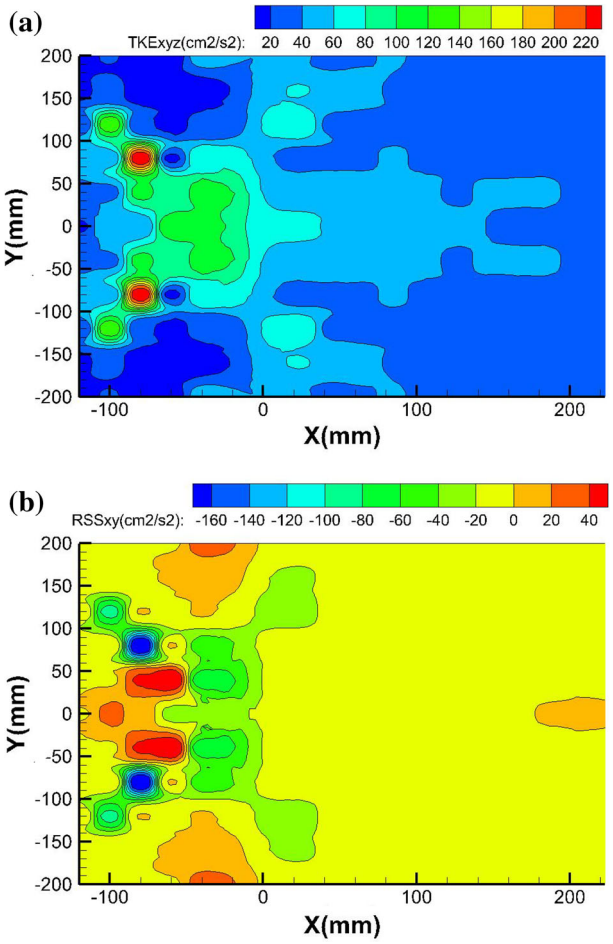

Fig. 7 Turbulent flow characteristics for movable bed: **a** Turbulent Kinetic Energy, **b** Reynolds shear stress

group of events in which their deflections are away from centreline and towards the sidewalls of the channel. Hence, each cluster of the bursting event consists of four types of the events including four internal events in cluster A and four external events in cluster B. Table 1 presents the internal and external events for flow at left side of the channel. For the right side of the channel the direction of transverse velocity fluctuation is mirrored (Fig. 3a). Therefore, for any point in the flow, eight different bursting events are defined here. The eight different types of bursting events and their associated flow characteristics have different influences on sediment particle entrainment from the bed of channel, and in particular around the bridge pier.

3.3 Inclination angle of the bursting events near the bed

The magnitude of forces applied to sediment particles at the bed is highly dependent on the inclination angle of the three-dimensional velocity fluctuations of the flow. Knowing the angle of attack of the bursting events is useful in understandingthe process of sediment

particle entainment from the bed [26,52,53,55]. In this section, the inclination angles of the eight orthogonal zones are presented for the fixed and movable bed experiments.

The inclination angle of the turbulent shear stress can be determined from

$$\theta_i = \left| \arctan\left(\frac{w'}{\sqrt{u'^2 - v'^2}} \right) \right| \tag{4}$$

where θ_i is angle of attack in the bursting class i from the horizontal plane, and u', v' and w' are fluctuating velocities in the streamwise, vertical and transverse directions, respectively. The inclination angle helps to find the direction of particle movements at the bed. Using Eq. (4) the inclination angle of bursting events in the eight orthogonal zones were computed for locations upstream of the pier and are presented in Figs. 8 and 9 for fixed and movable bed experiments, respectively. The results for the fixed bed experiment show that at a location 200 mm upstream of the pier, the inclination angles for internal ejection, internal sweep and external sweep events are higher than for outward and inward interactions. Hence, the stable sweep and ejection events apply forces at similar angles but in oposite directions, and it may be concluded that homogenous three-dimensional turbulence exists at this location. For the movable bed, at a location 40 mm upstream of the pier, where maximum scour occurred, the inclination angles for II-A, II-B, IV-A and IV-B are high, whereas for the outward and inward interactions, the maximum inclination angle is shifted to upstream locations. Additionally, for movable bed experiments, the results indicate that the angle of attack is larger than that for a fixed bed. Therefore, the magnitude of inclination angles for stable sweep and ejection events are higher than for other events particularly 40 mm upstream of the pier. As a result, the sediment entrainment regions are correspondingly correlated with the high magnitudes of inclination angles towards the bed.

3.4 Occurrence probability of the bursting events near the bed

The time fraction or occurrence probability of the eight orthogonal zones were computed based on the three velocity fluctuations. The time fraction of each event is necessary to calculate the occurrence probability of each event with respect to the sediment entrainment function. To estimate the probability of occurrence for each event, Keshavarzi and Gheisi [17] proposed the following equation:

$$P_k = \frac{n_k}{N} \tag{5}$$

$$N = \sum_{k=1}^{8} n_k \qquad k = 1, 2, 3, 4, 5..., 8 \tag{6}$$

where P_k is the occurence probability of each bursting event, n_k is the number of events in each class and N is the total number of bursting events. Using the above equations, the occurrence probabilities for the eight different bursting events were computed for locations upstream of the pier and are shown in Figs. 10 and 11 for the fixed and movable bed experiments, respectively.

The occurrence probabilities of the events at a location 40 mm upstream of the pier are 9, 16, 15, 9, 15, 9.5, 9.5 and 16%, respectively for I-A, II-A, III-A, IV-A, I-B, II-B, III-B and IV-B events (Fig. 10a–f). The highest occurrence probabilities are for II-A and IV-B events. The lowest occurrence probabilities are for I-A, IV-A, II-B and III-B events. For movable bed experiments, at the location where the maximum bed scouring occurred (Fig. 4a, b), the occurrence probabilities of the eight orthogonal zone are 6, 18, 8, 18, 8, 12, 7, and 24%,

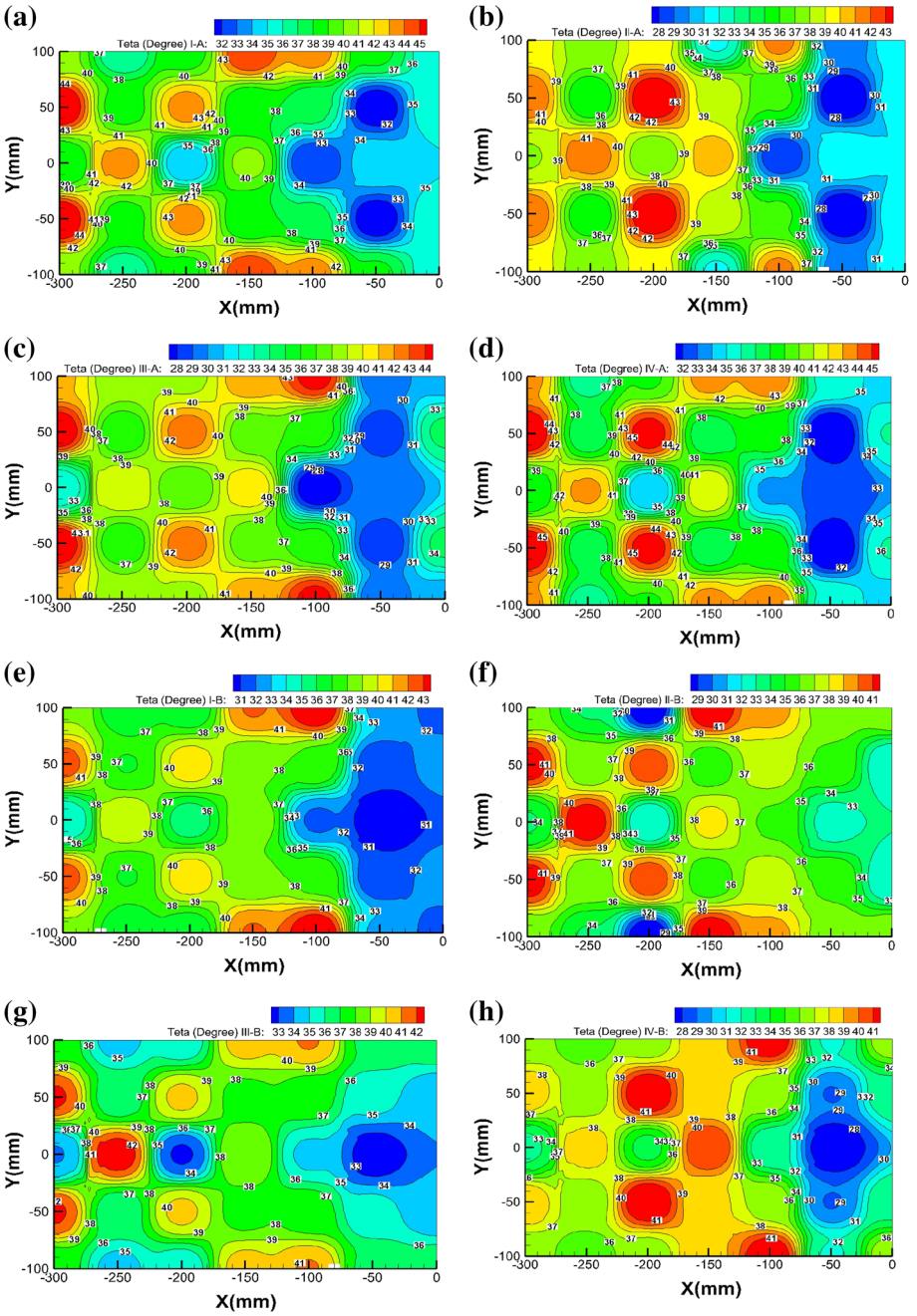

Fig. 8 The inclination angle of eight bursting events for fixed bed: **a** I-A, **b** II-A, **c** III-A, **d** IV-A, **e** I-B, **f** II-B, **g** III-B and **h** IV-B

respectively for I-A, II-A, III-A, IV-A, I-B, II-B, III-B and IV-B events (Fig. 11a–f). The results indicate that events II-A, and IV-B produced high occurrence probabilities, these contributing to the Reynolds shear stress at the bed and being consistent with the results for

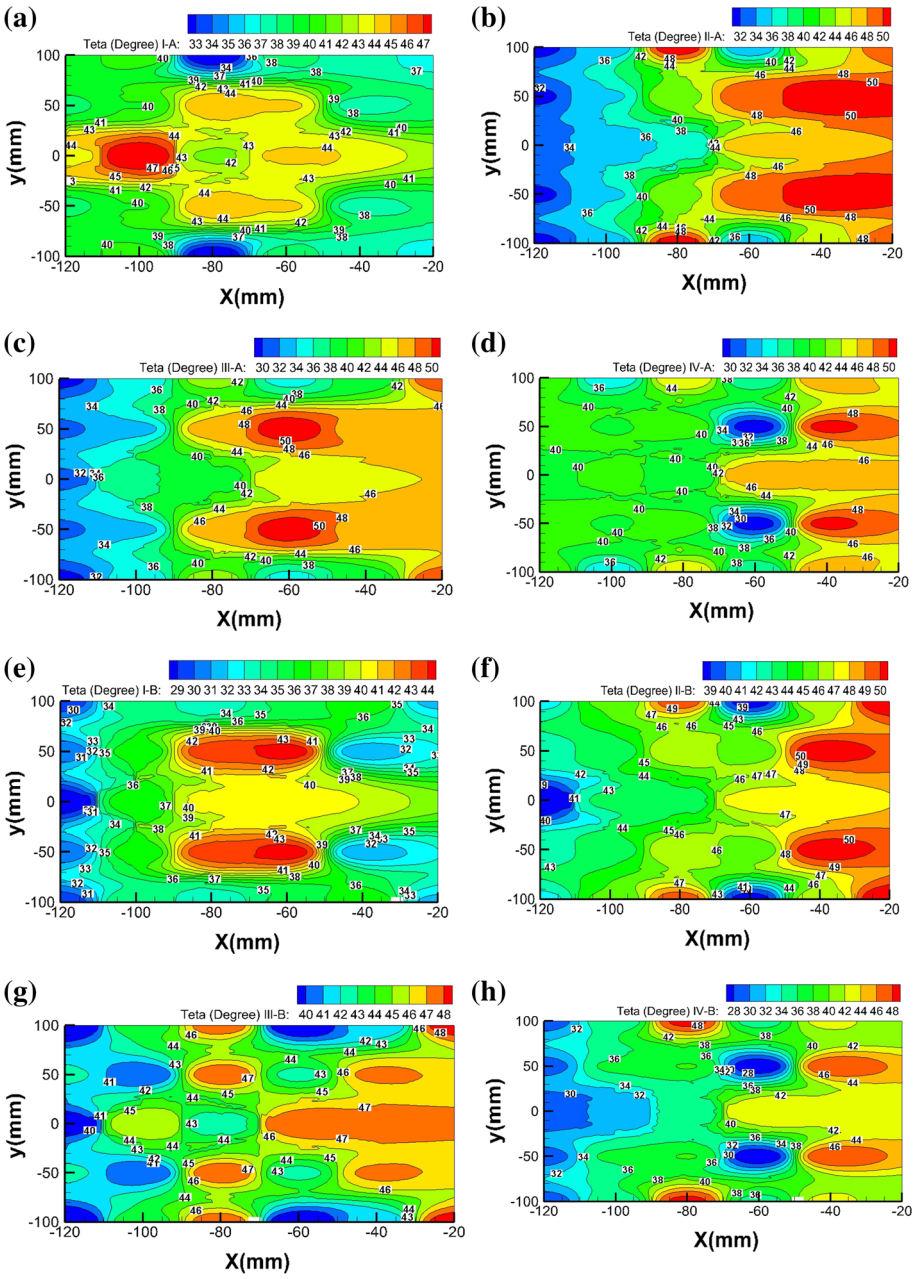

Fig. 9 The inclination angle of eight bursting events at movable bed: **a** I-A, **b** II-A, **c** III-A, **d** IV-A, **e** I-B, **f** II-B, **g** III-B and **h** IV-B

the movable bed. The lowest occurrence probabilities are found for I-A, III-A, I-B and III-B events. The above results demonstrate a high occurrence probability of three-dimensional bursting events inducing sediment movement.

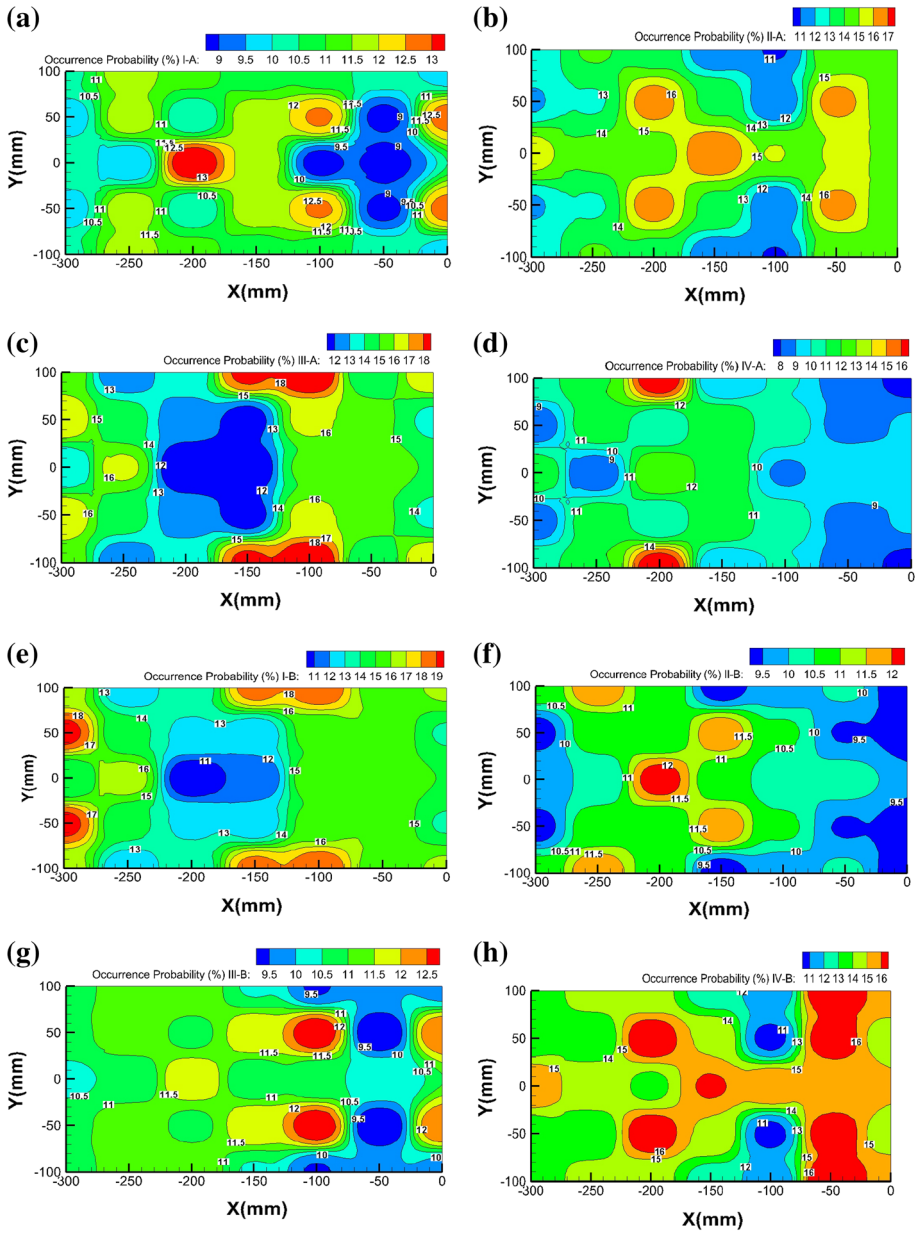

Fig. 10 The occurrence probability of eight bursting events at fixed bed: **a** I-A, **b** II-A, **c** III-A, **d** IV-A, **e** I-B, **f** II-B, **g** III-B and **h** IV-B

Occurrence frequency is the time fraction of the bursting events, as is highlighted by many previous researchers. For example, in octant analysis of the bursting process, eight occurrence probabilities of bursting events were recognized. However, the transition probabilities in octant analysis are categorized in 64 divisions (Fig. 12). Each division is the probability of movement from one state to another. It remains in one state or moves to another. The

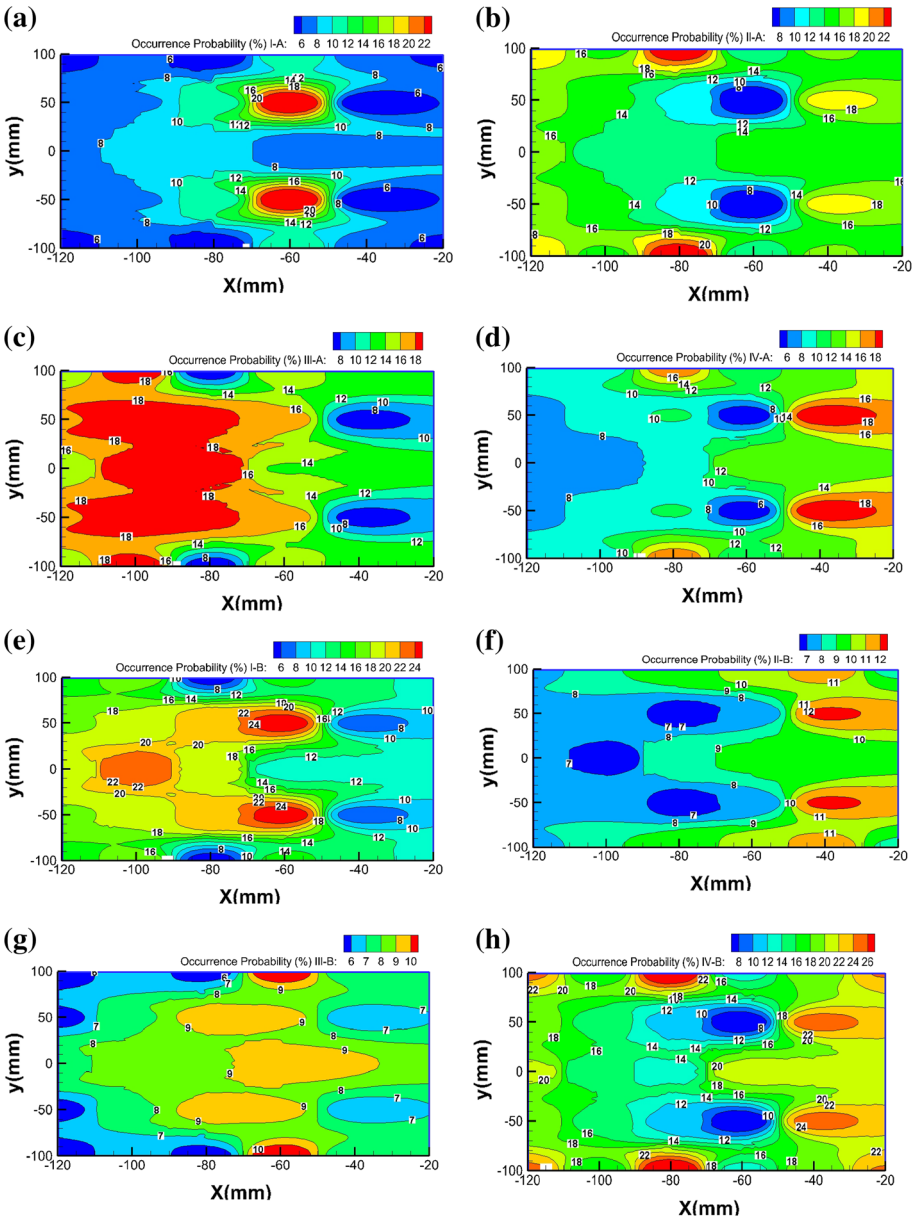

Fig. 11 The occurrence probability of eight bursting events at movable bed: **a** I-A, **b** II-A, **c** III-A, **d** IV-A, **e** I-B, **f** II-B, **g** III-B and **h** IV-B

occurrence probability does not consider the flow behaviour when it moves from one state to another. Therefore, occurrence probability itself cannot define the situation of bursting events. Transition probability provides information about the movement as well as the occurrence of the bursting events.

$$P(I)=\begin{vmatrix} P_{1\Rightarrow1} & P_{1\Rightarrow2} & P_{1\Rightarrow3} & P_{1\Rightarrow4} & P_{1\Rightarrow5} & P_{1\Rightarrow6} & P_{1\Rightarrow7} & P_{1\Rightarrow8} \\ P_{2\Rightarrow1} & P_{2\Rightarrow2} & P_{2\Rightarrow3} & P_{2\Rightarrow4} & P_{2\Rightarrow5} & P_{2\Rightarrow6} & P_{2\Rightarrow7} & P_{2\Rightarrow8} \\ P_{3\Rightarrow1} & P_{3\Rightarrow2} & P_{3\Rightarrow3} & P_{3\Rightarrow4} & P_{3\Rightarrow5} & P_{3\Rightarrow6} & P_{3\Rightarrow7} & P_{3\Rightarrow8} \\ P_{4\Rightarrow1} & P_{4\Rightarrow2} & P_{4\Rightarrow3} & P_{4\Rightarrow4} & P_{4\Rightarrow5} & P_{4\Rightarrow6} & P_{4\Rightarrow7} & P_{4\Rightarrow8} \\ P_{5\Rightarrow1} & P_{5\Rightarrow2} & P_{5\Rightarrow3} & P_{5\Rightarrow4} & P_{5\Rightarrow5} & P_{5\Rightarrow6} & P_{5\Rightarrow7} & P_{5\Rightarrow8} \\ P_{6\Rightarrow1} & P_{6\Rightarrow2} & P_{6\Rightarrow3} & P_{6\Rightarrow4} & P_{6\Rightarrow5} & P_{6\Rightarrow6} & P_{6\Rightarrow7} & P_{6\Rightarrow8} \\ P_{7\Rightarrow1} & P_{7\Rightarrow2} & P_{7\Rightarrow3} & P_{7\Rightarrow4} & P_{7\Rightarrow5} & P_{7\Rightarrow6} & P_{7\Rightarrow7} & P_{7\Rightarrow8} \\ P_{8\Rightarrow1} & P_{8\Rightarrow2} & P_{8\Rightarrow3} & P_{8\Rightarrow4} & P_{8\Rightarrow5} & P_{8\Rightarrow6} & P_{8\Rightarrow7} & P_{8\Rightarrow8} \end{vmatrix}$$

Fig. 12 Transition probability matrix of eight bursting events

3.5 Transition probability of three-dimensional bursting events

The probability of movement from a zone to the next zone with time is the focus of this study. It is assumed that in time step (t_i) in which $i = 1 \ldots n$, one event occurs in one of eight octant zones. The occurrence probability of an event after one time step (t_{i+1}) in the same zone, or in another zone can be determined using conditional probability analysis. Here, the conditional probability analysis was done using measured experimental data in statistical analysis; therefore it is called empirical conditional probability. At an instant of time, a discrete random variable represents an event in one of the eight octant zones I-A, II-A, III-A, IV-A, I-B, II-B, III-B and IV-B. A change in the situation or state of a time series event is defined as movement and can be investigated using the Markov process. A Markov process is governed by a set of probabilities, called transition probabilities. To investigate the state of bursting events, the organization of coherent turbulent flow was examined using an analysis of the transition probability, which is determined by conditional probability analysis [32].

With the application of the maximum likelihood estimators, the transition probabilities of first order Markov chain can be computed for time series of experimental data. A first order Markov process defines the current situation based only on the immediate past situation and can be expressed as:

$$pr\{s_{t+1}|s_t, s_{t-1}, \ldots, s_1\} = pr\{s_{t+1}|s_t\} \tag{7}$$

According to this concept, the probability of the next situation depends on the current situation, but it does not depend on the particular way that the model system arrived at the current situation. To find the transition probabilities of the movement of an event from one zone at time (t) to the next zone at time $(t+1)$, the following equation is used;

$$P_{i\to j} = \frac{n_{i\to j}}{n_i} \qquad i, j = 1.....8 \tag{8}$$

In Eq. (8), $P_{i\to j}$ is the movement probability of events from zone i at time (t) to zone j at time $(t+1)$, $n_{i\to j}$ is the number of movements of events in this way, and n_i is the number of events in the time series in zone i followed by another event. Based on the above concept, the probability of moving to the next state depends only on the current state, and does not depend on the way that the model system arrived at the current state. Here, transition probability is applied to find the probability of movement from one zone to another zone and, hence, 64 probable movements of three-dimensional bursting events are found. Figure 12 shows the matrix of transition probabilities for three dimensional bursting events.

Considering the matrix of transition probability, three specific possible movements were determined for two-dimensional quadrant analysis of bursting events [32]. For three-

dimensional analysis of the bursting process the organized coherent structures are classified as marginal movement, cross movement and stable movement: **Marginal movement** is defined as the marginal or lateral movement of bursting events that may occur if an event moves to the neighbouring zones, for example, zones I-A $\leftrightarrow$ I-B, I-A $\leftrightarrow$ II-B and I-A2 $\leftrightarrow$ IV-A (Fig. 2b). Compared to other organizations, these movements are relatively weak. **Cross movement** is the transition between the crossed zones, for example between zone I-A $\leftrightarrow$ III-A and I-A $\leftrightarrow$ III-B (Figure 2b). This organization is the weakest organization when compared to other movements. **Stable movement** occurs when an event in time step t_i and t_{i+1} stays in the same zone (Fig. 2b). The stable transition probabilities of the internal and external events are defined as $P(ij)$, where $i = j$. For example, the stable transition probabilities of internal and external sweep events are $P(i = \text{IV-A}, j = \text{IV-A})$ and $P(i = \text{IV-B}, j = \text{IV-B})$, respectively. Therefore, the event has stability in transition due to stability in its situation and it does not have a tendency to move to the other zones.

The computed 64 transition probabilities of bursting events are listed in Table 3 for measured experimental data at two locations downstream of the pier. The results in Table 3 indicate that the probability of stable organization is higher than others. In other words, when an event occurs at time step t_i in one of the zone, the probability of the event to stay in the same zone at time step $t_i + 1$ is higher than other organizations. The transition probabilities of I-A $\Rightarrow$ I-A, II-A $\Rightarrow$ II-A, III-A $\Rightarrow$ III-A, IV-A $\Rightarrow$ IV-A, I-B $\Rightarrow$ I-B, II-B $\Rightarrow$ II-B, III-B $\Rightarrow$ III-B and IV-B $\Rightarrow$ IV-B are higher than other movements. The above results are in agreement with the reported transition probabilities in previous studies [17,52,53]. Additionally, at line B for the location 65 mm downstream from the pier, the maximum transition probabilities of $(P(ij) = 65.7, 61.2\,\%)$ were found for zones II-A $\Rightarrow$ II-A and IV-B $\Rightarrow$ IV-B, respectively (highlighted in italic). At Line C for location 65 mm downstream, maximum values of transition probability were found to be 68.1 and 66.8 % for II-A $\Rightarrow$ II-A and IV-B $\Rightarrow$ IV-B, respectively (highlighted in italic). The transition probabilities for other movements are very low when compared with the stable transition probabilities. Therefore in this study, only the variation of stable transition probabilities and their relevance on sediment entrainment are investigated.

The variation of stable transition probabilities for eight zones are shown in Fig. 13a–c for lines A, B and C, respectively. The results in Fig. 13a–c indicate that the transition probability values for II-A and IV-B are higher than those for the other zones. Additionally the average transition probabilities in the transverse direction are presented in Fig. 14 for fixed bed and movable bed. The results indicate that the transition probabilities for II-A and IV-B are higher than other events from upstream to downstream of the pier. In Fig. 15, the comparison of the average transition probabilities at upstream of the pier are shown for fixed and movable beds. In Figs. 14 and 15b, the locations in which stable events occur with approximately similar transition probability are areas with isotropic turbulence region [53,56].

3.6 Transition probability of bursting events and sediment movement

In this study, new insights using three-dimensional behaviour of turbulent flow around bridge piers in open channels are investigated. The important implementation challenge with using three-dimensional analysis of bursting events is seeking the probability that a sediment particle will move around a bridge pier in the next time step given the current condition. To address this challenge, the transition probability of a bursting event must be determined. An important question here is how stable events are distributed within the flow around the bridge pier respective to the bed scouring pattern. Additionally, there is always a question that, if at a particular time step, the bursting event is in a particular zone, what is the situation at the

Table 3 The transition probability matrix of eight bursting events along lines B and C downstream of pier

	(I-A) $t+\Delta t$	(II-A) $t+\Delta t$	(III-A) $t+\Delta t$	(IV-A) $t+\Delta t$	(I-B) $t+\Delta t$	(II-B) $t+\Delta t$	(III-B) $t+\Delta t$	(IV-B) $t+\Delta t$	Sum
Line B (65mm)									
(I-A)t	**51.9**	17.6	4.4	14.0	7.2	1.6	0.3	2.8	100
(II-A)t	12.0	*65.7*	13.0	3.7	0.8	3.5	0.6	0.6	100
(III-A)t	2.0	15.1	**57.6**	12.9	0.3	1.8	7.4	2.9	100
(IV-A)t	9.7	3.7	14.1	**45.8**	3.7	0.5	4.9	17.4	100
(I-B)t	6.5	2.5	0.5	2.4	**57.8**	13.6	2.6	14.0	100
(II-B)t	3.1	15.4	1.3	0.7	14.9	**49.6**	10.9	4.1	100
(III-B)t	1.2	2.9	7.3	2.7	5.9	14.3	**51.1**	14.7	100
(IV-B)t	0.8	0.6	1.6	5.6	14.1	4.7	11.3	*61.2*	100
Line C (65mm)									
(I-A)t	**46.6**	17.5	4.9	17.5	7.4	1.9	0.5	3.5	100
(II-A)t	10.3	*68.1*	14.2	3.2	0.8	2.0	1.0	0.4	100
(III-A)t	3.4	19.7	**53.2**	11.0	0.3	1.7	8.2	2.5	100
(IV-A)t	13.0	5.2	13.6	**40.7**	2.4	0.8	4.8	19.6	100
(I-B)t	6.2	2.9	0.4	2.6	**54.8**	13.0	2.0	18.0	100
(II-B)t	2.9	17.3	3.3	1.5	12.4	**48.1**	11.7	2.9	100
(III-B)t	0.5	4.0	6.5	1.9	3.5	17.2	**49.4**	17.0	100
(IV-B)t	1.4	0.1	1.4	3.2	13.8	3.8	9.6	*66.8*	100

next time step. A sweep event may be followed by an inward interaction event or another sweep event. The question is that which of these subsequent events have a greater effect of sediment entrainment.

To compare transition probabilities distribution with the scouring pattern around a bridge pier (Figure 4b), the contour lines of transition probabilities of eight bursting events for fixed bed and the scoured bed are presented in Figs. 16 and 17, respectively. In Figs 16 and 17, only the information for a strip of 100 mm is presented. The pattern of the information in Figures 16 and 17 shows an organized distribution of transition probabilities. For the fixed bed (Fig. 16), the eight events have approximately the same transition probabilities from −300 to −150 mm. However, a high gradient of transition probabilities was observed from −150 to 0 mm, where the horseshoe vortex and down flow occur [11,14,57]. Close to the pier, where the down flow is strongest, there exists a high gradient of transition probabilities for internal sweep, external sweep and internal ejection events (Figs. 16a–c, 17a–c). The patterns of transition probability for internal outward interaction events (Fig. 16e) appears to only have a minor role in sediment entrainment as those forces result in the force vector being directed towards the water surface [20]. The high value of transition probabilities for the internal and external inward interaction events (Fig. 16g) indicate a backward flow mechanism which appears to not be effective for particle entrainment as the force vectors is directed opposite to the mean flow direction. Figure 17a–c indicate that internal sweep and external sweep events direct the flow towards the bed and can thereby entrain sediment particles. The internal sweep is directed towards the centreline of the flume, thus increasing the scour activity near the pier, while the external sweep moves particles away from the centreline towards the side walls (Figs. 17 a, b and 1b). The internal ejection also moves sediment particles away from the scour hole (Fig. 17c). Comparing the pattern of transition

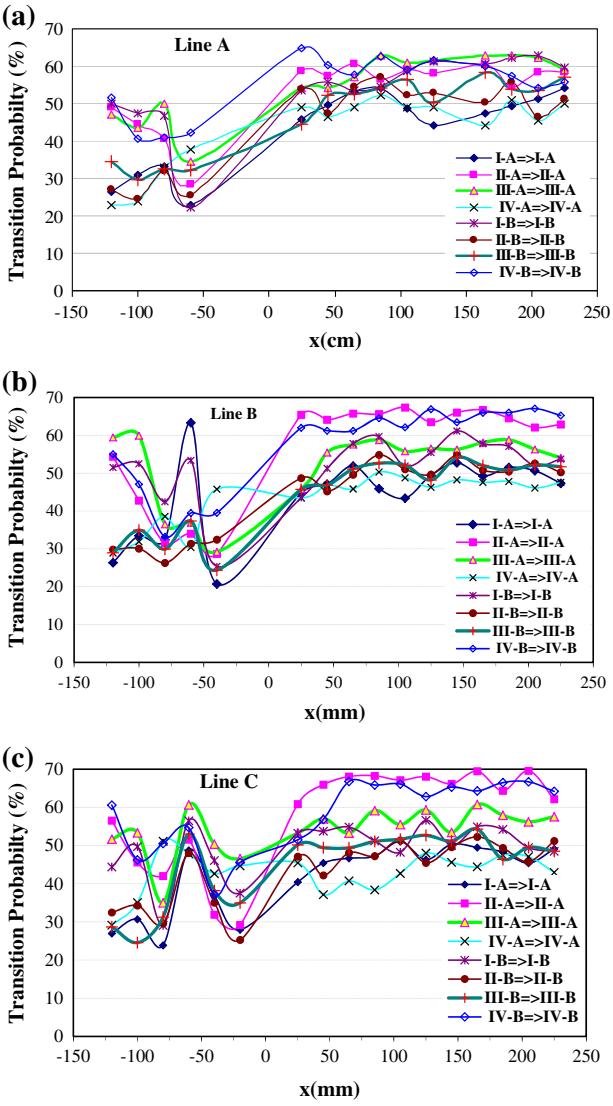

Fig. 13 Transition probabilities of eight stable zones at **a** line A, **b** Line B and **c** Line C

probabilities for internal and external sweeps, consistency can be found with the scouring pattern. The effect of external outward interaction (Fig. 17f) may be misinterpreted as it is directed parallel to the streamwise flow direction and therefore needs to be investigated in more detail.

In Fig. 17a–h, the maximum transition probabilities were external sweep and internal ejection events with probabilities of 66 and 68 %, respectively, while the transition probabilities of internal sweep and external ejection events are 50 and 56 %, respectively. The results are in agreement with the findings from fixed bed experiments. Hence it can be concluded that

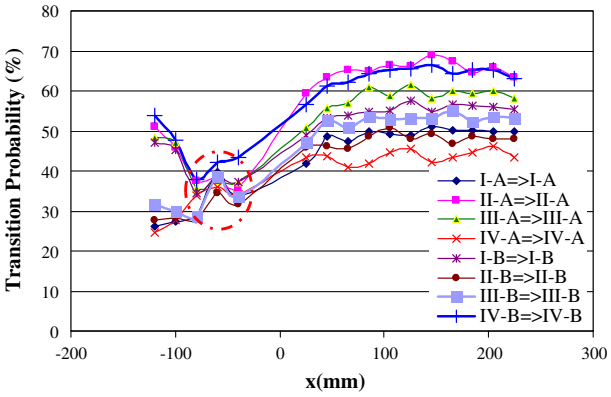

Fig. 14 Average stable transition probabilities in transverse direction for eight stable events for movable bed

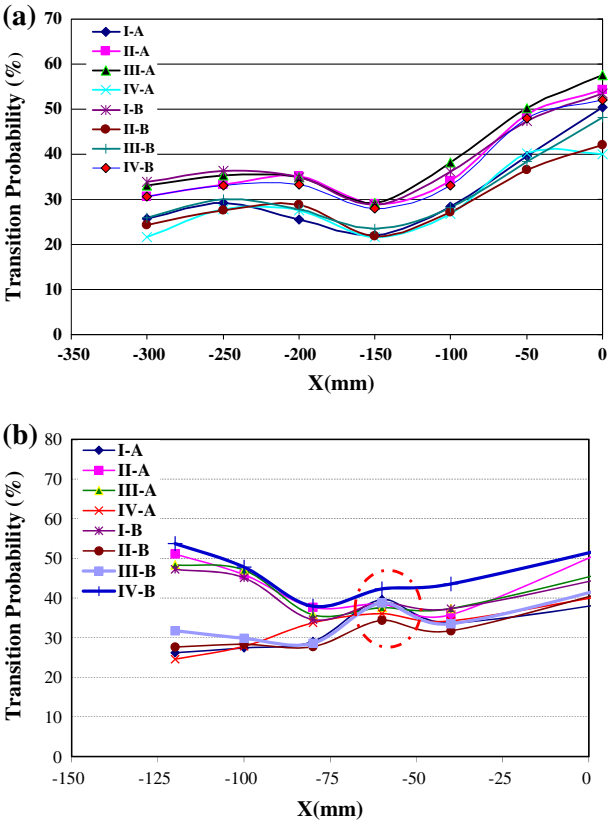

Fig. 15 Averaged transverse stable transition probabilities in upstream of pier for **a** fixed bed and **b** movable bed

the internal sweep pushing force towards bed and external ejection diverts sediment particles away from centreline.

Behind the pier, a corridor of external sweep and internal ejection events is observed in the middle of the channel downstream of the pier. This is due to the wake behind the

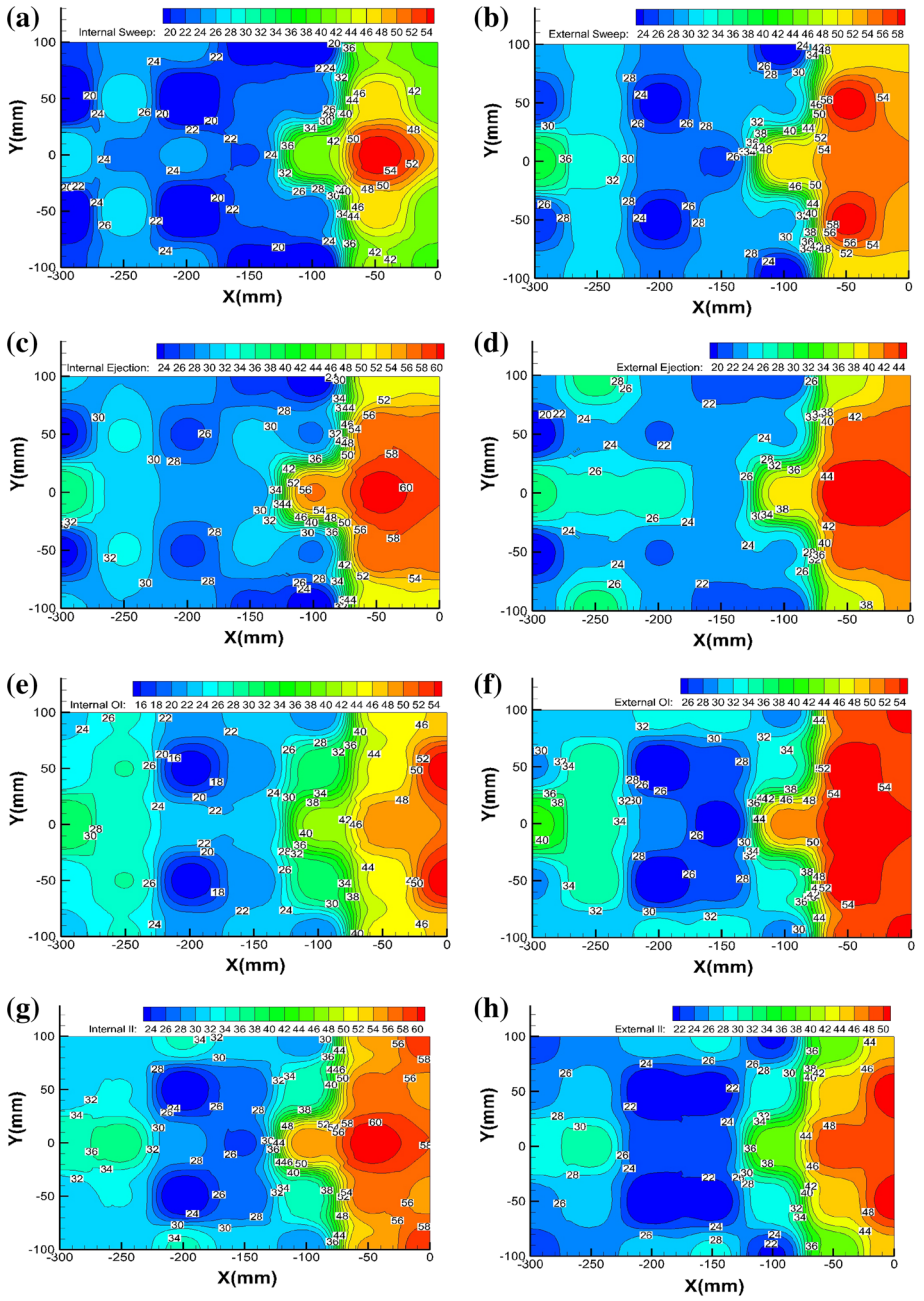

Fig. 16 Contour lines of the stable transition probability for fixed bed upstream of pier: **a** internal sweep events; **b** External sweep event, **c** internal ejection events, **d** external ejection event, **e** internal outward interaction events, **f** external outward interaction events, **g** internal inward interaction events, **h** external inward interaction events

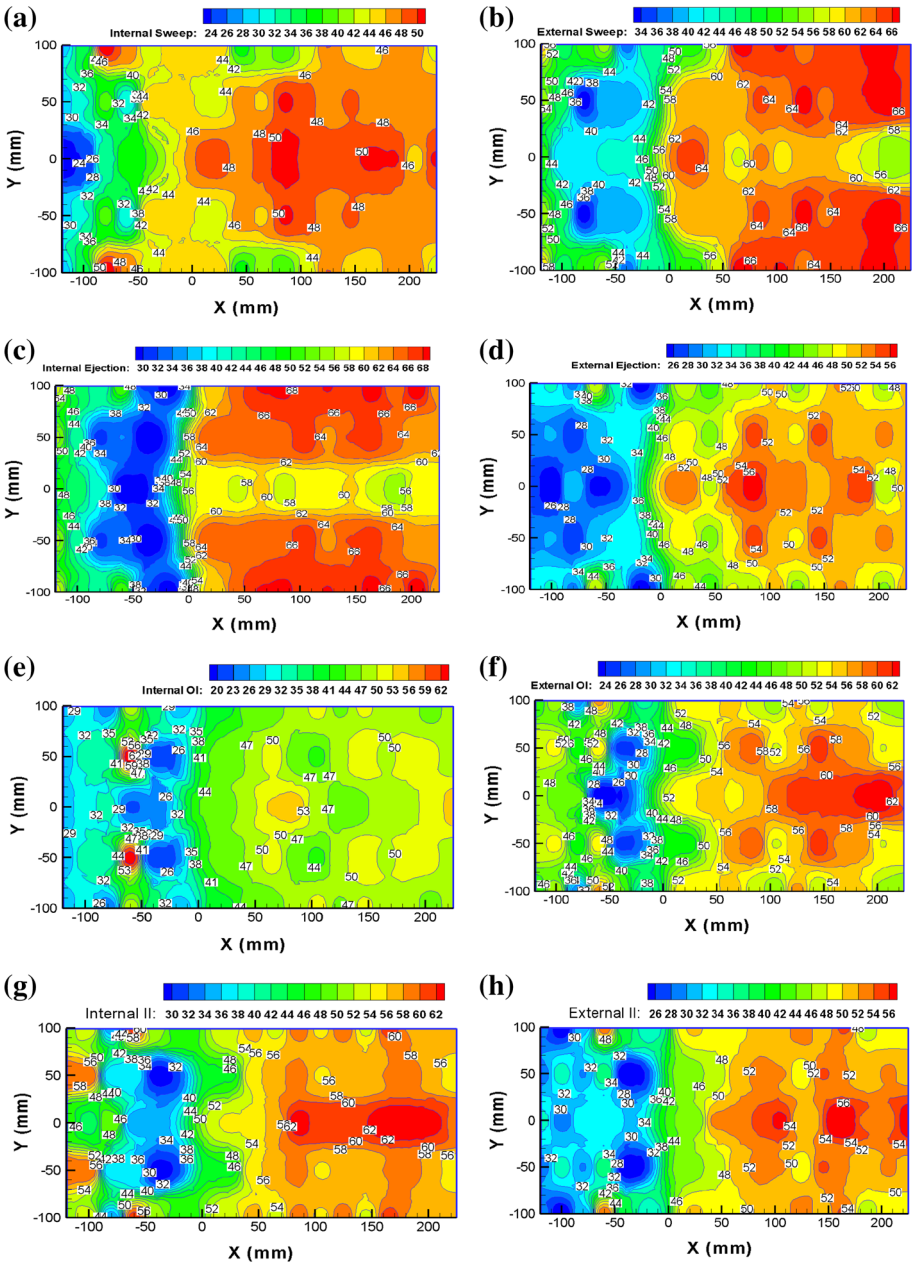

Fig. 17 Contour lines of the stable transition probability for movable bed upstream and downstream of pier: **a** internal sweep events, **b** external sweep event, **c** internal ejection events, **d** external ejection event, **e** internal outward interaction events, **f** external outward interaction events, **g** internal inward interaction events, **h** external inward interaction events

bridge pier. As it can be seen, stable transition probabilties of external sweep and internal ejection events have similar probabilities at the centre-line and at the sides of the channel (Fig. 17b, c). Downstream of the bridge pier, stable transition probabilty of external sweep

and internal ejection events shows a trailing vortex formed at both side of the pier. The trailing wake vortex system of strong turbulence forms a necklace vortex and spreads transversally at the rear of the pier (Fig. 17b, c). The above results are in agreement with the finding from previous studies [6,8,46]. A higher value of transition probability was found for external sweep and internal ejection events at a distance equal to 1.2 times of the pier diameter from the center-line of the channel. The above results are in agreement with the findings of Kumar and kothyari [57] for the principal vortex.

The three-dimensional analysis of bursting events presented herein can be used to predict the direction of sediment movement near the bed around a cylindrical bridge pier. This technique is an effective technique to analyse three-dimensional flow. The results are consistent with the bed topography generated around the bridge pier and provide more resolution to the understanding of coherent flow structure and bursting processes. The above findings are in agreement with the reported results in previous studies [51–53]. The above results are promising for development of a technique with better resolution for flow structure analysis. However, to generalize the results, more experiments must be done under different flow conditions.

4 Conclusion

Three-dimensional bursting analysis was undertaken to identify the most likely coherent flow structure events in the vicinity of a cylindrical bridge pier with a developed scour hole. The 64 transition probabilities of the bursting events occurring in the corresponding eight zones were determined from experimental data. It was found that external sweep and internal ejection events have the highest transition probabilities when compared to other events. The results also indicate that the transition probability of external sweep, internal sweep and internal ejection events are in phase with the bed profile especially on lines A, B and C, which span the scour region from upstream to downstream of the pier. The average transition probabilities of the events for lines A, B, C are higher for II-A and IV-B than for the other events. The transition probabilities for the stable events decreased from upstream to downstream of the pier. The maximum decrease occurred for II-B, while the minimum decrease occurred for IV-A. Also it is shown that higher transition probability occurred during the external sweep and internal ejection events indicating that they are effective in promoting sediment entrainment around a single circular bridge pier.

References

1. Lu JY, Shi ZZ, Hong JH, Lee JJ, Raikar RV (2011) Temporal variation of scour depth at nonuniform cylindrical piers. J Hydraul Eng 137(1):45–56
2. Melville BW, Coleman SE (2000) Bridge scour. Water Resources Publications, Highlands Ranch
3. Richardson E.V., Davies S.R. (1995) Evaluating scour at bridges. Rep. No. FHWAIP-90-017 (HEC 18), Federal Highway Administration, U.S. Department of Transportation, Washington, D.C
4. Chang WY, Lai JS, Yen CL (2004) Evolution of scour depth at circular bridge piers. J Hydraul Eng 130(9):905–913
5. Raudkivi AJ, Ettema R (1983) Clear water scour at cylindrical piers. J Hydraul Eng 109(3):338–349
6. Tsutsui T (2008) Fluid force acting on a cylindrical pier standing in a scour. Bluff Bodies Aerodynamics & Applications, Milano, Italy, BBAA VI International Colloquium, July 20–24
7. Melville BW, Chiew YM (1999) Time scale for local scour at bridge piers. J Hydraul Eng 125(1):59–65
8. Morton B.R., Evans-Lopez J.L. (1986) Horseshoe vortices and bridge pier erosion. 9th Australian Fluid Mechanics Conference, Auckland, 8–12 December

9. Kirkil G, Constantinescu G (2008) Coherent structures in the flow field around a circular cylinder with scour hole. J Hydraul Eng 134(5):572–587
10. Dargahi B (1989) The turbulent flow field around a circular cylinder. Exp Fluids 8:1–12
11. Melville BW, Raudkivi AJ (1977) Flow characteristics in local scour at bridge piers. J Hydraul Res 15(1):373–380
12. Ettema R, Kirkil G, Muste M (2006) Similitude of large-scale turbulence in experiments on local scour at cylinders. J Hydraul Eng 132(1):33–40
13. Sumer BM, Fredsoe J (2002) The mechanics of scour in the marine environment. World Scientific, London
14. Unger J, Hager WH (2007) Down flow and horseshoe vortex characteristics of sediment embedded bridge piers. Exp Fluids 42:1–19
15. Kline SJ, Reynolds WC, Schraub FA, Runstadler PW (1967) The structure of turbulent boundary layers. J Fluid Mech 30(4):741–743
16. Hussain AKMF (1983) Coherent structures: reality and myth. Phys Fluids 26:2816–2838
17. Keshavarzi A, Gheisi AR (2006) Stochastic nature of three-dimensional bursting events and sediment entrainment in vortex chamber. J Stochast Environ Res Risk Assess 21(1):75–87
18. Offen GR, Kline SJ (1975) A proposed model of the bursting process in turbulent boundary layers. J Fluid Mech 70:209–228
19. Roy AG, Buffin-Belanger T, Lamarre H, Kirkbride AD (2004) Size, shape and dynamics of large-scale turbulent flow structures in a gravel-bed river. J Fluid Mech 500:1–27
20. Ganapathisubramani B, Hutchins N, Hambleton WT, Longmire EK, Marusic I (2005) Investigation of large-scale coherence in a turbulent boundary layer using two-point correlations. J Fluid Mech 524:57–80
21. Wohl EE (2000) Mountain rivers. American Geophysical Union, Washington, DC
22. Dey S, Bose SK, Sastry GLN (1995) Clear water scour at circular piers: a model. J Hydraul Eng 121(12):869–876
23. Thorne PD, Williams JJ, Heathershaw AD (1989) In situ acoustic measurements of marine gravel threshold and transport. Sedimentology 36:61–74
24. Townsend AA (1976) The structure of turbulent shear flow. Cambridge University Press, Cambridge
25. Nezu I, Nakagawa H (1993) Turbulence in open-channel flows, International Association for Hydraulic Research (IAHR). Rotterdam, Netherlands
26. Bridge JS, Bennett SJ (1992) A model for entrainment and transport of sediment grains of mixed sizes, shapes and densities. Water Resour Res 28(2):337–363
27. Keshavarzi A, Ball JE (1997) An analysis of the characteristics of rough bed turbulent shear stress in an open channel flow. J Stochast Hydrol Hydraul 11(3):193–210
28. Nakagawa H, Nezu I (1977) Prediction of the contributions to the Reynolds stress from bursting events in open-channel flows. J Fluid Mech 80(1):99–128
29. Grass AJ (1971) Structural features of turbulent flow over smooth and rough boundaries. J Fluid Mech 50(2):233–255
30. Nychas SG, Hershey HC, Brodkey RS (1973) A visual study of turbulent shear flow. J Fluid Mech 61:513–540
31. Keshavarzi A, Ball J, Nabavi H (2012) Frequency pattern of turbulent flow and sediment entrainment over ripples using image processing. Hydrol Earth Syst Sci 16:147–156. doi:10.5194/hess-16-147
32. Keshavarzi A., Shirvani A. (2002) Probability analyses of instantaneous shear stress and entrained particles from the bed, CSCE/EWRI of ASCE Environmental Engineering Conference, Niagara Falls
33. Nelson JM, Shreve RL, Mclean SR, Drake TG (1995) Role of near-bed turbulence structure in bed load transport and bed form mechanics. Water Resour Res 31(8):2071–2086
34. Drake TG, Shreve RL, Dietrich WE, Whiting PJ, Leopold LB (1988) Bed load transport of fine gravel observed by motion picture photography. J Fluid Mech 192:193–217
35. Keshavarzi A, Ball JE (1999) An application of image processing in the study of sediment motion. J Hydraul Res 37(4):559–576
36. Cuthbertson AJS, Ervine DA (2005) Experimental study of fine particle settling in turbulent open channel flows over rough porous beds. J Hydraul Eng 133(8):905–916
37. Marchioli C, Soldati A (2002) Mechanisms for particle transfer and segregation in a turbulent boundary layer. J Fluid Mech 468:283–315
38. Dwivedi A, Melville B, Shamseldin AY (2010) Hydrodynamic forces generated on a spherical sediment particle during entrainment. J Hydraul Eng 136(10):756–769
39. Dwivedi A, Melville B, Shamseldin AY, Guha TK (2011) Flow structures and hydrodynamic force during sediment entrainment. Water Resour Res 47:W01509. doi:10.1029/2010WR009089
40. Raudkivi AJ (1998) Loose boundary hydraulics. A. A Balkema, Rotterdam, The Netherlands
41. Sontek ADV Operation Manual (1997) Firmware version 4.0. Sontek, San Diego.

42. Goring DG, Nikora VI (2002) Despiking acoustic Doppler velocimeter data. J Hydraul Eng 128(1):117–126
43. Wahl T (2002) Discussion on despiking acoustic Doppler velocimeter bata by Goring and Nikora. J Hydraul Eng 129(6):484–487
44. Dargahi B (1990) Controlling mechanism of local scouring. J Hydraul Eng 116(10):1197–1214
45. Devenport WJ, Simpson RL (1990) Time-dependent and time averaged turbulence structure near the nose of a wing-body junction. J Fluid Mech 210:23–55
46. Simpson RL (2001) Junction flows. Annu Rev Fluid Mech 33:415–443
47. Graf WH, Istiarto I (2002) Flow pattern in the scour hole around a cylinder. J Hydraul Res 40(1):13–20
48. Duan JG, He L, Wang GQ, Fu XD (2011) Turbulent bursts around an experimental spur dike. Int J Sedim Res 26(4):471–486
49. Jafari Mianaei S, Keshavarzi A (2008) Spatio-temporal variation of transition probability of bursting events over the ripples at the bed of open channel. J Stoch Environ Res Risk Assess 22(2):257–264
50. Jafari Mianaei S, Keshavarzi A (2010) Study of near bed stochastic turbulence and sediment entrainment over the ripples at the bed of open channel using image processing technique. J Stoch Environ Res Risk Assess 24(5):591–598
51. Papanicolaou AN, Diplas P, Evaggelopoulos N, Fotopoulos S (2002) Stochastic incipient motion criterion for spheres under various bed packing conditions. J Hydraul Eng 128(4):369–380
52. Esfahani F, Keshavarzi A (2011) Effect of different meander curvatures on spatial variation of coherent turbulent flow structure inside ingoing multi-bend river meanders. Stoch Environ Res Risk Assess 25:913–928
53. Esfahani F, Keshavarzi A (2013) Dynamic mechanism of turbulent flow in meandering channels: considerations for deflection angle. Stoch Environ Res Risk Assess 27:1093–1114
54. Liu X, Bai Y (2013) Three-dimensional bursting phenomena in meander channel. Trans Tianjin Univ 19:17–24
55. Breusers HNC, Nicollet G, Shen HW (1977) Local scour around cylindrical piers. J Hydraul Res 15(3):211–252
56. Keshavarzi A (1997) Entrainment of sediment particles from a fixed bed with the influence of near-wall turbulence. PhD Thesis, University of New South Wales, Australia.
57. Kumar A, Kothyari UC (2012) Three-Dimensional flow characteristics within the scour hole around circular uniform and compound piers. J Hydraul Eng 138(5):420–429